JOURNAL OF THEORETICAL
AND APPLIED MECHANICS
43, 2, pp. 257-275, Warsaw 2005

NUMERICAL ANALYSIS OF VERTICAL ROTOR DYNAMICS OF ACWW 1000 CENTRIFUGE

JANUSZ ZACHWIEJA

Faculty of Mechanical Engineering, University of Technology and Agriculture
email: jz@zmp.com.pl

KRZYSZTOF LIGIER

Faculty of Technical Sciences, University of Warmia and Mazury in Olsztyn
email: klig@uwm.edu.pl

In this work, a numerical approach to analysis of dynamics of a hung rotor has been presented. A vertical rotor of the ACWW 1000 centrifuge has been used as a real object for verification of the discussed model. This rotor, due to its constructional features, should show the gyroscopic effect in the range of achievable rotational speed.

Key words: gyroscopic effect, natural frequency, Campbell diagram

1. Introduction

Centrifuges are high-speed machines whose rotor disks are most frequently situated on a vertical shaft. Such a design allows one to eliminate the disadvantageous influence of the potential asymmetry of the disk or the shaft on machine dynamics, which is revealed by the occurrence of the so called critical speed of the second kind (Gryboś, 1994).

Due to significant angular rotational speed, even slight unbalance can cause vibrations with significant velocity and shift amplitudes (Zachwieja, 2002b). In the case of high slenderness shafts, the gyroscopic effect is of big importance (Zachwieja, 2002a; Sawicki and Genta, 2000). In some designs, this effect is forced by a special method of supporting the rotor. Concurrent precession causes self-centering of the shaft after exceeding the critical speed of the second kind. This phenomenon is known as the "de Laval effect" (Gosiewski and Muszyńska, 2000).

Vibrations of rotors as continuous systems used to be the subject of many studies both analytical (Awrejcewicz and Krysko, 2000) and numerical ones (Nelson and McVaugh, 1976), which include the anisotropy of the first and second kind (Zachwieja, 2004; Mohiuddin and Khulief, 1999; Jei and Lee, 1993; Kang *et al.*, 1997).

This work is an example of numerical analysis of vibrations of a vertical axis centrifuge combined with experimental verification of the achieved results.

2. Numerical analysis of rotor free vibrations

The ACWW 1000 rotor is used in the sugar industry. As a crucial element of the sugar crystallization process line, it was the subject of tests performed in order to identify its critical unserviceable states (Mikołajczak and Ligier, 2003). The exterior of the device and its interior are shown in Fig. 1.

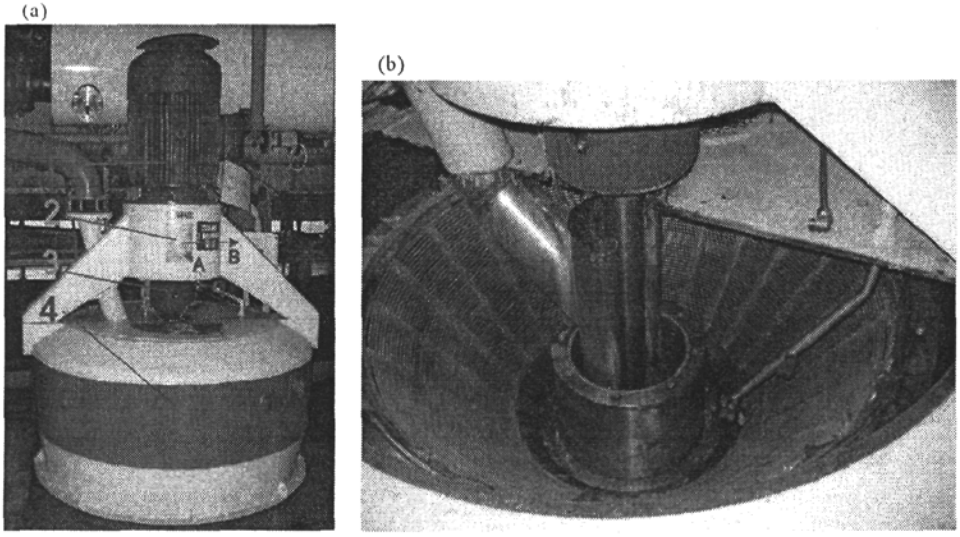

Fig. 1. (a) ACWW 1000 rotor, 1 engine, 2 bearing housing, 3 clutch, 4 barrel housing; (b) view of the centrifuge interior

The movable element is the engine (1) – clutch (2) – barrel (6) system. It can be considered that way because of the length of the shaft on which the barrel is set, when it is 1200 mm, and its diameter 70 mm, whereas the rotational speed is 1800 rpm. Then the influence of the gyroscopic effects on the rotor dynamics should be noticeable. This system is similar to the rotor

model with a hung disk, however, the classic Green-Stodola's model assumes that the disk possesses an infinitely high stiffness, which, for obvious reasons, is significant simplification of real conditions. However, this assumption enables relatively easy use of the finite element method in the description of dynamics of both the shaft and the disk.

2.1. Shaft dynamics

The shaft is most frequently modeled by the so called beam elements, i.e. elements with four degrees of freedom in the node. This means that we take into consideration only the possibility of occurrence of shaft flexural vibrations, thus neglecting the influence of torsional ones as well as the action of axial forces. Such a simplification does not exactly corresponds with real conditions as the elementts are also subject to torsion and thus torsional vibrations.

On the other hand, bearing in mind that free vibrations of the torsional character occur with frequencies higher than flexural vibrations, the introduced simplifications enable one formulate a matrix of inertia, stiffness and damping in a simple form guaranteeing that obtained calculation results are found with a small error.

The node displacement vector components $\boldsymbol{\delta}_w$ are four shifts and four angles (Fig. 2)

$$\boldsymbol{\delta}_S = [u_i, w_i, \psi_i, \theta_i, u_j, w_j, \psi_j, \theta_j]^\top \tag{2.1}$$

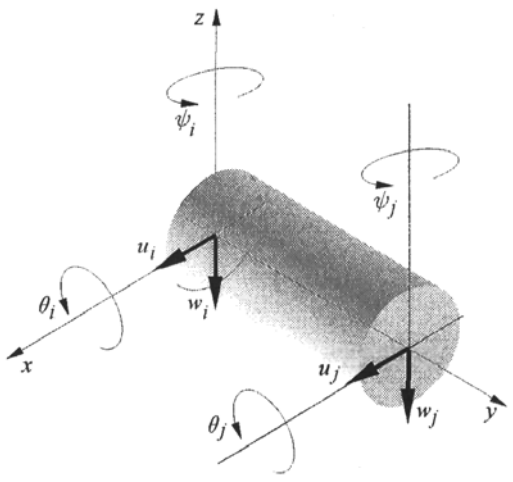

Fig. 2. A deformable finite element of the shaft with four degrees of freedom in the node

The displacements and the deflection angles of the element are expressed as follows

$$\begin{bmatrix} u(y) \\ w(y) \end{bmatrix} = \mathbf{N}(y)\boldsymbol{\delta}_S \tag{2.2}$$

and

$$\begin{bmatrix} \psi(y) \\ \theta(y) \end{bmatrix} = \begin{bmatrix} -\dfrac{\partial u(y)}{\partial y} \\ \dfrac{\partial w(y)}{\partial y} \end{bmatrix} = \begin{bmatrix} -1 & 0 \\ 0 & 1 \end{bmatrix} \mathbf{D}(y)\boldsymbol{\delta}_S \tag{2.3}$$

here

$$\mathbf{N}(\xi) = \begin{bmatrix} N_{11} & 0 & N_{13} & 0 & N_{15} & 0 & N_{17} & 0 \\ 0 & N_{22} & 0 & N_{24} & 0 & N_{26} & 0 & N_{28} \end{bmatrix} \tag{2.4}$$

where

$$\begin{aligned} N_{11} &= N_{22} = 1 - 3\xi^2 + 2\xi^3 \\ -N_{13} &= N_{24} = L\xi(1 - 2\xi + \xi^2) \\ N_{15} &= N_{26} = 3\xi^2 - 2\xi^3 \\ -N_{17} &= N_{28} = L(-\xi^2 + \xi^3) \end{aligned}$$

is the matrix of the finite element shape function, whereas the matrix $\mathbf{D}$ is expressed by the relationship

$$\mathbf{D}(\xi) = \frac{1}{L}\frac{\partial}{\partial \xi}\mathbf{N} = \frac{1}{L}\begin{bmatrix} D_{11} & 0 & D_{13} & 0 & D_{15} & 0 & D_{17} & 0 \\ 0 & D_{22} & 0 & D_{24} & 0 & D_{26} & 0 & D_{28} \end{bmatrix} \tag{2.5}$$

where

$$\begin{aligned} -D_{11} &= D_{15} = -D_{22} = D_{26} = 6\xi - 6\xi^2 \\ -D_{13} &= D_{24} = L(1 - 4\xi + 3\xi^2) \\ -D_{17} &= D_{28} = L(-2\xi + 3\xi^2) \end{aligned}$$

The coordinate y, referred to the infinite element length, is marked with

$$\xi = \frac{y}{L} \tag{2.6}$$

The shaft is axi-symmetrical, it does not show any " inner anisotropy" features. Since it performs rotation about it, it is convenient to consider its displacements in a movable system $Ox'y'z'$ connected with it. The relation between the movable and the permanent system is expressed by Euler's angles

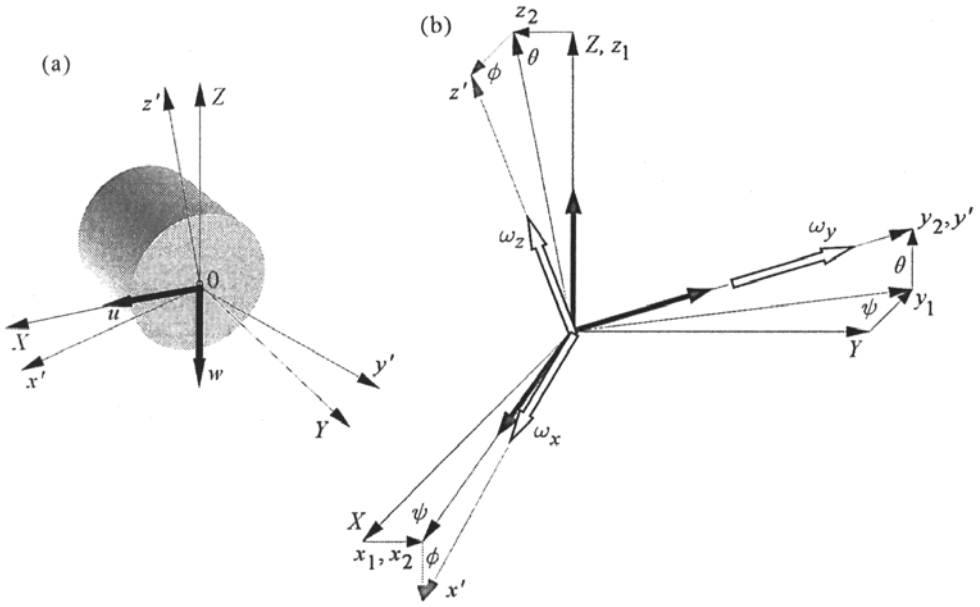

Fig. 3. (a) Reference systems used for dynamical analysis of the asymmetrical shaft; (b) reference systems used for description of rotation of the centrifuge shaft

ϕ, θ, ψ. We can assume that the angles θ, ψ are small, whereas the angular velocity $\dot{\phi}$ is the shaft rotational speed. It will be marked by Ω.

The system $OXYZ$ shifts to the location of $Ox'y'z'$ during three rotations with respect to the appropriate axes

- rotation around the axis Z by the angle ψ
- rotation around the axis x_1 by the angle θ
- rotation around the axis y_2 by the angle ϕ.

Instantaneous angular velocity of the section in the system $0x'y'z'$ has the following components

$$\begin{aligned}
\omega_x &= \dot{\psi}\cos\Big(\frac{\pi}{2}+\phi\Big) + \dot{\theta}\cos\phi = \dot{\theta}\cos\phi - \dot{\psi}\sin\phi \\
\omega_y &= \dot{\psi}\cos\Big(\frac{\pi}{2}-\theta\Big) + \dot{\phi} = \dot{\psi}\theta + \dot{\phi} \\
\omega_z &= \dot{\psi}\cos\phi + \dot{\theta}\cos\Big(\frac{\pi}{2}-\phi\Big) = \dot{\theta}\sin\phi + \dot{\psi}\cos\phi
\end{aligned} \tag{2.7}$$

Kinetic energy of the shaft element is the sum of its translatory and rotary components

$$E_S = \frac{1}{2}\rho A \int_0^L (\dot{u}^2 + \dot{w}^2)\, dy + \frac{1}{2}\rho I \int_0^L (\omega_x^2 + 2\omega_y^2 + \omega_z^2)\, dy \tag{2.8}$$

where

$\omega_x, \omega_y, \omega_z$	–	angular velocities expressed by (2.7)
$I_x = I_z = I$	–	geometrical inertia moments of the element section with respect to the principal axes x' and z'
$I_y = I_x + I_z = 2I$	–	inertia moment of the element cross-section with respect to the axis y
A, L, ρ	–	area of the cross-section, length, density of the element, respectively
u, w	–	translatory displacements of the shaft.

From the second term of (2.8), we can additionally separate the element

$$E_{Sg} = \rho I_y \Omega \int_0^L \dot{\psi}\theta\, dy = 2\rho\Omega I \int_0^L \dot{\psi}\theta\, dy \tag{2.9}$$

which is kinetic energy of the shaft element corresponding to precession (gyroscopic effect)

$$E_{Si} = \rho I \int_0^L \Omega^2\, dy \tag{2.10}$$

which is kinetic energy of the shaft element due to rotation (does not depend on the generalized coordinates)

$$E_{Sr} = \frac{1}{2}\rho I \int_0^L (\dot{\theta}^2 + \dot{\psi}^2)\, dy \tag{2.11}$$

which is kinetic energy due to angular motions of the shaft.

If we neglect the strain resulting from shear, the energy of the elastic strain caused by bending is expressed by

$$U_S = \frac{1}{2} \int_0^L EI\Big[\Big(\frac{\partial^2 u}{\partial y^2}\Big)^2 + \Big(\frac{\partial^2 w}{\partial y^2}\Big)^2\Big]\, dy \tag{2.12}$$

The virtual work of the force of gravity of the shaft element is performed along the virtual displacement δw. Thus, it assumes the form

$$\delta L_S = -g \int_0^L \rho A \delta w \, dy = \tag{2.13}$$

$$= -\rho g A \Big(\delta w_1 \int_0^L N_1 \, dy + \delta \theta_1 \int_0^L N_2 \, dy + \delta w_2 \int_0^L N_3 \, dy + \delta \theta_2 \int_0^L N_4 \, dy \Big)$$

For formulating equations of motion of the shaft element, we use Lagrange'a equations of the II kind

$$\frac{d}{dt}\Big(\frac{\partial E_S}{\partial \dot{\boldsymbol{\delta}}_S}\Big) - \frac{\partial E_S}{\partial \boldsymbol{\delta}_S} + \frac{\partial (U_S + L_S)}{\partial \boldsymbol{\delta}_S} = 0 \tag{2.14}$$

The determination of matrices:

— inertia during translatory motion

$$\mathbf{M}_{St} = \rho A \int_0^L \mathbf{N}^{\top} \mathbf{N} \, dy = \tag{2.15}$$

$$= \frac{\rho A L}{420} \begin{bmatrix} 156 & 0 & -22L & 0 & 54 & 0 & 13L & 0 \\ 0 & 156 & 0 & 22L & 0 & 54 & 0 & -13L \\ -22L & 0 & 4L^2 & 0 & -13L & 0 & -3L^2 & 0 \\ 0 & 22L & 0 & 4L^2 & 0 & 13L & 0 & -3L^2 \\ 54 & 0 & -13L & 0 & 156 & 0 & 22L & 0 \\ 0 & 54 & 0 & 13L & 0 & 156 & 0 & -22L \\ 13L & 0 & -3L^2 & 0 & 22L & 0 & 4L^2 & 0 \\ 0 & -13L & 0 & -3L^2 & 0 & -22L & 0 & 4L^2 \end{bmatrix}$$

— inertia during rotation

$$\mathbf{M}_{Sr} = \rho I \int_0^L \mathbf{D}^{\top} \mathbf{D} dy = \frac{\rho I}{30L} \begin{bmatrix} 36 & 0 & -3L & 0 & -36 & 0 & -3L & 0 \\ 0 & 36 & 0 & 3L & 0 & 36 & 0 & 3L \\ -3L & 0 & 4L^2 & 0 & 3L & 0 & -L^2 & 0 \\ 0 & 3L & 0 & 4L^2 & 0 & -3L & 0 & -L^2 \\ -36 & 0 & 3L & 0 & 36 & 0 & 3L & 0 \\ 0 & 36 & 0 & -3L & 0 & 36 & 0 & -3L \\ -3L & 0 & -L^2 & 0 & 3L & 0 & 4L^2 & 0 \\ 0 & 3L & 0 & -L^2 & 0 & -3L & 0 & 4L^2 \end{bmatrix} \tag{2.16}$$

— gyroscopic

$$\mathbf{G}_S = \rho I \int_0^L \mathbf{D}^\top \begin{bmatrix} 0 & -1 \\ 1 & 0 \end{bmatrix} \mathbf{D}\, dy = \tag{2.17}$$

$$= \frac{\rho I}{30L} \begin{bmatrix} 0 & -36 & 0 & -3L & 0 & 36 & 0 & -3L \\ 36 & 0 & -3L & 0 & -36 & 0 & -3L & 0 \\ 0 & 3L & 0 & 4L^2 & 0 & -3L & 0 & -L^2 \\ 3L & 0 & -4L^2 & 0 & -3L & 0 & L^2 & 0 \\ 0 & 36 & 0 & 3L & 0 & -36 & 0 & 3L \\ -36 & 0 & 3L & 0 & 36 & 0 & 3L & 0 \\ 0 & 3L & 0 & -L^2 & 0 & -3L & 0 & 4L^2 \\ 3L & 0 & L^2 & 0 & -3L & 0 & -4L^2 & 0 \end{bmatrix}$$

is only the question of proper transformations of dependence (2.14). Moreover, by denoting

$$\mathbf{B} = \frac{\partial^2}{\partial y^2}\mathbf{N} = \frac{1}{L^2} \begin{bmatrix} -\frac{6}{L}a_1 & 0 & -a_2 & 0 & \frac{6}{L}a_1 & 0 & -a_3 & 0 \\ 0 & -\frac{6}{L}a_1 & 0 & a_2 & 0 & \frac{6}{L}a_1 & 0 & a_3 \end{bmatrix} \tag{2.18}$$

where

$$a_1 = 1 - 2\xi \qquad a_2 = -4 + 6\xi \qquad a_3 = -2 + 6\xi$$

we obtain, from the differentiation of the potential energy with respect to $\boldsymbol{\delta}_S$, an expression for the stiffness matrix of the shaft element

$$\boldsymbol{K}_S = EI_m \int_0^L \mathbf{B}^\top \mathbf{B}\, dy = \tag{2.19}$$

$$= \frac{EI}{L^3} \begin{bmatrix} 12 & 0 & -6L & 0 & -12 & 0 & -6L & 0 \\ 0 & 12 & 0 & 6L & 0 & -12 & 0 & 6L \\ -6L & 0 & 4L^2 & 0 & 6L & 0 & 2L^2 & 0 \\ 0 & 6L & 0 & 4L^2 & 0 & -6L & 0 & 2L^2 \\ -12 & 0 & 6L & 0 & 12 & 0 & 6L & 0 \\ 0 & -12 & 0 & -6L & 0 & 12 & 0 & -6L \\ -6L & 0 & 2L^2 & 0 & 6L & 0 & 4L^2 & 0 \\ 0 & 6L & 0 & 2L^2 & 0 & -6L & 0 & 4L^2 \end{bmatrix}$$

2.2. Disk dynamics

For the purposes of the analysis of the stiff disk dynamics we assume that its mass center overlaps the center of the shaft elastic section. The disk nodal displacement vector has the following form

$$\boldsymbol{\delta}_D = [u_o, w_o, \psi_o, \theta_o]^\top \tag{2.20}$$

The dynamics of the symmetric disk motion is considered in reference systems analogical to those for the shaft $OXYZ$, $0'x'y'z'$ (Fig. 4). The disk kinetic energy can be expressed as

$$E_D = \frac{1}{2}m(\dot{u}_o^2 + \dot{w}_o^2) + \frac{1}{2}[J(\omega_x^2 + \omega_z^2) + 2J\omega_y^2] \tag{2.21}$$

where

$\omega_x, \omega_y, \omega_z$	–	angular velocity vector components of the disk rotary motion
$J_z = J_x = J, J_y = 2J$	–	mass inertia moments of the disk
m	–	disk mass
u_o, w_o	–	displacement of the disk mass center.

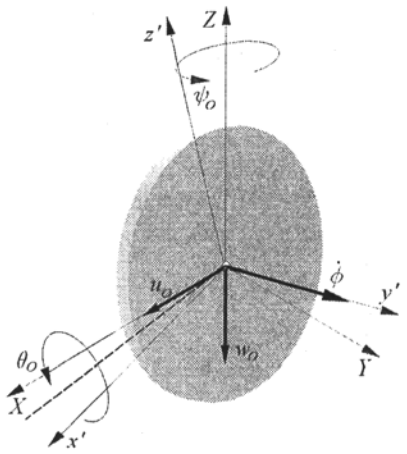

Fig. 4. The modeling of the disk in the OES method

Equations (2.7) derived for the shaft also refer to a disk set in the shaft. Therefore, we can show an expression for the disk kinetic energy in the following way

$$E_D = \frac{1}{2}m(\dot{u}_o^2 + \dot{w}_o^2) + 2J\Omega\dot{\psi}_o\theta_o + J\Omega^2 + \frac{1}{2}J(\dot{\theta}_o^2 + \dot{\psi}_o^2) \tag{2.22}$$

The physical meaning of particular terms in expression (2.22) is analogical to that of the shaft.

Having expressed the dependence for kinetic energy by generalized coordinates, we can define matrices occurring in the equation of motion of the disk found by making use of Lagrange's equations. Thus

$$\mathbf{M}_D = \begin{bmatrix} m & 0 & 0 & 0 \\ 0 & m & 0 & 0 \\ 0 & 0 & J & 0 \\ 0 & 0 & 0 & J \end{bmatrix} \qquad \mathbf{G}_D = \begin{bmatrix} 0 & 0 & 0 & 0 \\ 0 & 0 & 0 & 0 \\ 0 & 0 & 0 & J \\ 0 & 0 & -J & 0 \end{bmatrix} \tag{2.23}$$

2.3. Free vibrations

Free vibrations of the rotor, whose mathematical model has been presented in Sections 2.1-2.2, are described by general equations

$$\mathbf{M}^G_{S,D}\ddot{\boldsymbol{\delta}} + 2\Omega\mathbf{G}^G_D\dot{\boldsymbol{\delta}} + \mathbf{K}^G_S\boldsymbol{\delta} = \mathbf{0} \tag{2.24}$$

Here, $\mathbf{M}^G_{S,D}$ is the global inertia matrix created from local inertia matrices of finite elements of the shaft and the disk. $\mathbf{G}^G_D$ denotes the global gyroscopic matrix of disks when we accept the gyroscopic effect as being the only damping factor and neglecting the internal damping. $\mathbf{K}^G_S$ defines the global stiffness matrix of the shaft elements. In this model, the disk is an element which is infinitely stiff and its mass is many times bigger than the mass of the shaft.

The issue of free vibrations of the immovable rotor reduces (2.24) to the form

$$\mathbf{M}^G_{S,D}\ddot{\boldsymbol{\delta}} + \mathbf{K}^G_S\boldsymbol{\delta} = \mathbf{0} \tag{2.25}$$

The solution to this equation has the form

$$\boldsymbol{\delta} = \boldsymbol{\delta}_0 \exp(-\mathrm{i}\omega t) \tag{2.26}$$

whereas $\boldsymbol{\delta}_0$ is an eigenvector, and ω describes natural frequencies. These values are determined as characteristic roots ($\omega = \sqrt{\lambda}$) of the equation obtained from the matrix eigenvalue problem

$$[\mathbf{K}^G_S]^{-1}\mathbf{M}^G_{S,D} - \lambda\mathbf{I} = \mathbf{0} \tag{2.27}$$

The equation of free vibration of the shaft elements including the gyroscopic effect has the form

$$\mathbf{M}^G_{S,D}\ddot{\boldsymbol{\delta}} + 2\Omega\mathbf{G}^G_D\dot{\boldsymbol{\delta}} + \mathbf{K}^G_S\boldsymbol{\delta} = \mathbf{0} \tag{2.28}$$

In order to find the solution to the problem of matrix eigenvalues, we substitute

$$\boldsymbol{y} = \begin{bmatrix} \dot{\boldsymbol{\delta}} \\ \boldsymbol{\delta} \end{bmatrix} \qquad \dot{\boldsymbol{y}} = \begin{bmatrix} \ddot{\boldsymbol{\delta}} \\ \dot{\boldsymbol{\delta}} \end{bmatrix} \tag{2.29}$$

Equation (2.28) can be then alternatively written as

$$\begin{bmatrix} \mathbf{0} & \mathbf{M}_{S,D}^{G} \\ \mathbf{M}_{S,D}^{G} & 2\Omega\mathbf{G}_{D}^{G} \end{bmatrix} \begin{bmatrix} \ddot{\boldsymbol{\delta}} \\ \dot{\boldsymbol{\delta}} \end{bmatrix} - \begin{bmatrix} \mathbf{M}_{S,D}^{G} & \mathbf{0} \\ \mathbf{0} & -\mathbf{K}_{S}^{G} \end{bmatrix} \begin{bmatrix} \dot{\boldsymbol{\delta}} \\ \boldsymbol{\delta} \end{bmatrix} = \begin{bmatrix} \mathbf{0} \\ \mathbf{0} \end{bmatrix} \tag{2.30}$$

Multiplying (2.30) by the matrix

$$\begin{bmatrix} [\mathbf{M}_{S,D}^{G}]^{-1} & \mathbf{0} \\ \mathbf{0} & -[\mathbf{K}_{S}^{G}]^{-1} \end{bmatrix}$$

pne arrivesat the following simplification

$$\begin{bmatrix} \mathbf{0} & \mathbf{I} \\ -[\mathbf{K}_{S}^{G}]^{-1}\mathbf{M}_{S,D}^{G} & -[\mathbf{K}_{S}^{G}]^{-1}2\Omega\mathbf{G}_{D}^{G} \end{bmatrix} \dot{\boldsymbol{y}} - \mathbf{I}\boldsymbol{y} = \mathbf{0} \tag{2.31}$$

If we substitute

$$\boldsymbol{y} = \boldsymbol{\delta}_0 e^{st} = \boldsymbol{\delta}_0 \exp[(\alpha + \mathrm{i}\omega)t] \tag{2.32}$$

where α is the damping exponent, ω – free vibration frequency, we obtain an equation

$$\Big(\boldsymbol{A} - \frac{1}{s}\mathbf{I}\Big)\boldsymbol{\delta}_0 = \mathbf{0} \tag{2.33}$$

being the searched one in the eigenproblem of the matrix $\mathbf{A}$

$$\mathbf{A} = \begin{bmatrix} \mathbf{0} & \mathbf{I} \\ -[\mathbf{K}_{S}^{G}]^{-1}\mathbf{M}_{S,D}^{G} & -[\mathbf{K}_{S}^{G}]^{-1}2\Omega\mathbf{G}_{D}^{G} \end{bmatrix} \tag{2.34}$$

Here, $\beta_i = 1/s_i$ denote successive eigenvalues, whereas δ_{0_i} are the eigenvectors corresponding to them.

Since the real shape of the rotor is quite complicated (Fig. 5a), the idea of its simplification down to the model basing on the concept of a deformable shaft and infinitely stiff disk, whose dynamics was described in Sections 2.1 and 2.2, seems to be worth considering. Therefore, a simplified model (Fig. 5b) with similar masses and inertia moments of disks and the shaft is proposed.

According to the accepted procedure, the rotor shaft is digitized with finite elements of the beam type and the disks are treated as elements of infinitely

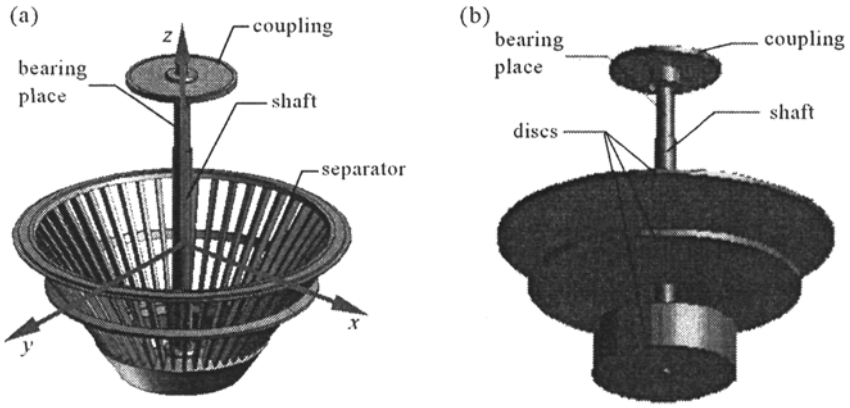

Fig. 5. (a) The ACWW 1000 centrifuge rotor; (b) simplified model of the rotor

big stiffness at the same time. Due to lack of available data concerning actual stiffness of the bearings, the support is selected in such a way that it assumes their low flexibility.

Table 1. Physical features of the rotor and the substitute model

			Rotor	Substitute model	error [%]
Shaft	m	kg	30.92	30.92	0
	J_{xx}	kg mm^2	3.023E+6	3.023E+6	0
	J_{yy}	kg mm^2	3.023E+6	3.023E+6	0
	J_{zz}	kg mm^2	1.719E+4	1.719E+4	0
Coupling	m	kg	18.78	20.43	8.87
	J_{xx}	kg mm^2	1.464E+5	1.491E+5	2.12
	J_{yy}	kg mm^2	1.464E+5	1.491E+5	2.12
	J_{zz}	kg mm^2	2.802E+5	2.808E+5	0.21
Separator	m	kg	203.23	202.60	−0.31
	J_{xx}	kg mm^2	2.002E+7	1.995E+7	−0.35
	J_{yy}	kg mm^2	2.002E+7	1.995E+7	−0.35
	J_{zz}	kg mm^2	2.832E+7	2.483E+7	−12.3

In Fig. 6 the first four free vibration frequencies of the immovable rotor as well as the corresponding modal forms obtained from equations (2.28)-(2.34) are presented.

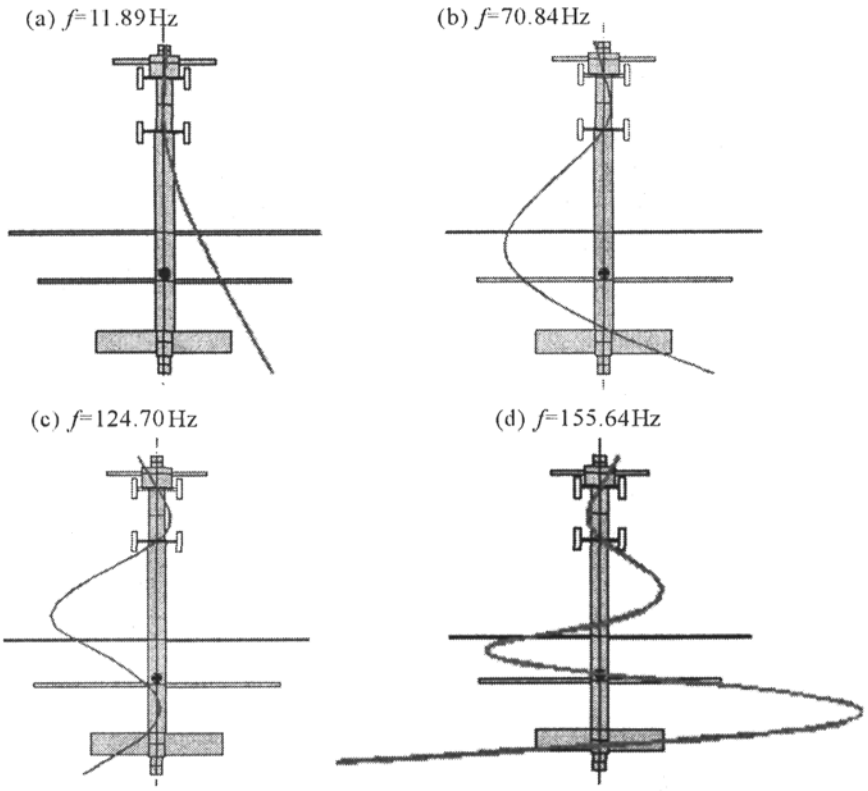

Fig. 6. The first four natural frequencies and corresponding forms of the simplified model

For the purposes of comparison, natural frequencies of the rotor vibrations based on a 3D model truly reflecting the rotor size and its material features have been numerically determined. In calculations that have been carried out with the use of the MSC NASTRAN program, infinite beam elements of the tetragonal type have been used. The results are presented in Fig. 7.

The comparison of the results obtained for both models enables one to notice that they differ significantly, even in the case of the first resonance frequency. According to the accepted assumption concerning the simplified model, one obtains solutions corresponding neither with the rotor longitudinal vibrations nor vibrations of the disk itself.

2.4. Gyroscopic effect

The method of the shaft support by bearings and the way the disc is being hung should cause noticeable precession of the rotor. The influence of

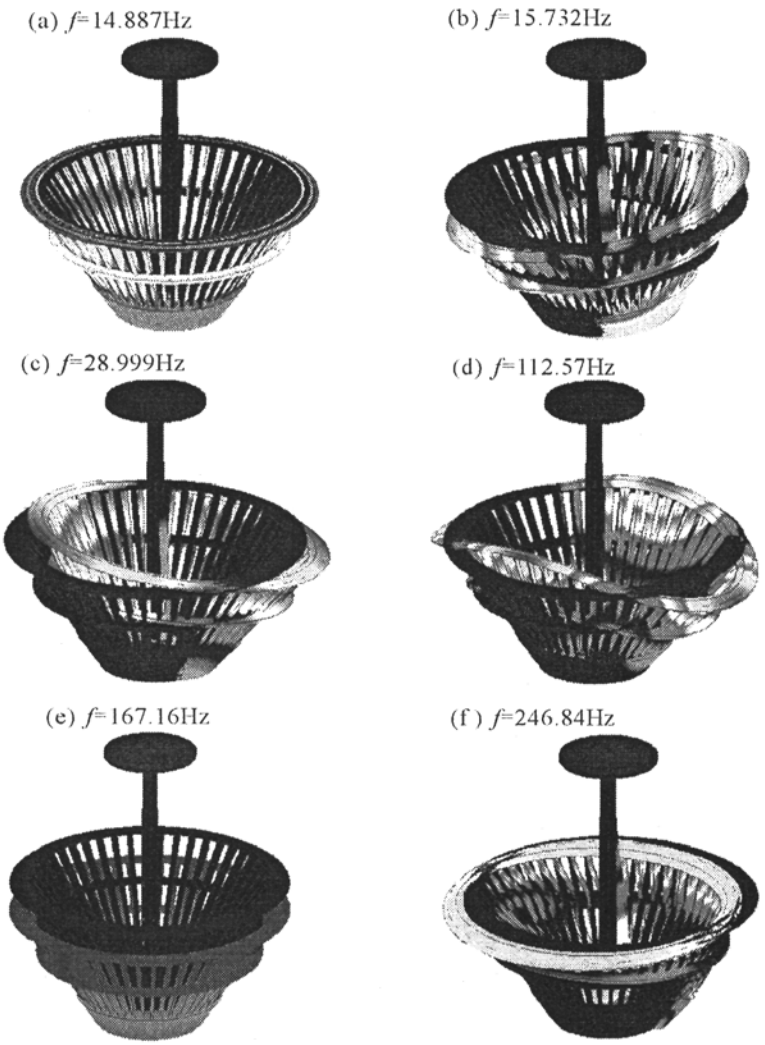

Fig. 7. The first six natural frequencies and corresponding modes of the rotor

the gyroscopic effect on free vibration frequencies of the simplified model is presented in Campbell's diagram. It has been made for rotational speeds within the range 0-10000 rpm.

It confirms the assumption that even for the range of rotational speeds within which the centrifuge operates, the influence of gyroscopic effects should be significant. In Fig. 9, hypothetic changes of the rotor free vibration frequencies (left column) under the influence of the gyroscopic moment (right column) at the rotational speed 1800 rpm are presented. The term "hypothetic" comes

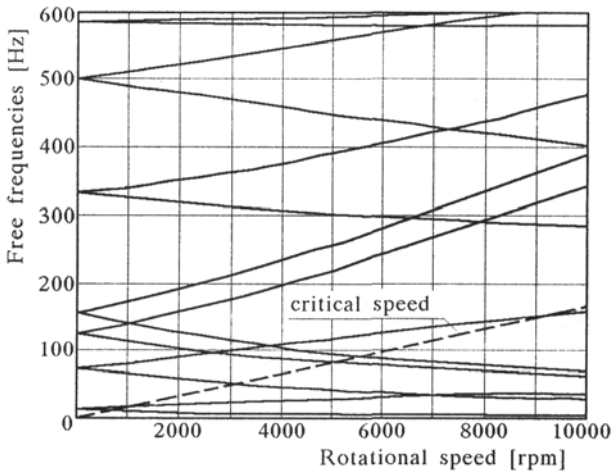

Fig. 8. Campbell's diagram for the analysed rotor model

from the fact that it is not possible to predict whether during real rotor motion there will exist conditions for the occurrence of backward precession or whether rotation of the rotor with a revolving disk will be of a concurrent character.

3. Conclusions

In order to verify the results of numerical calculation for both models, vibrations of three ACCW1000 centrifuges have been analysed. Precession measurements were realised with the use of roto-current transformers measuring shaft deflection during one rotation. Test results are presented in Fig. 10. It can be seen that in none of the cases the maximum shaft deflection exceeds the value of 0.15 mm. Bearing in mind the fact that operational clearences in bearings can even reach the value of 0.1 mm it should be thought that the gyroscopic moment is not of much significance for the strained rotor axis within the applied rotational speeds.

On the resonance curve obtained from measurements of the rotor effective vibration while it is running up to the velocity 1800 rpm, the maximum values corresponding with frequencies 19 Hz and 29 Hz are clearly marked. They are close to the values of calculated free vibration frequencies corresponding with successive forms of flexural vibrations of the rotor at rest. It means that the influence of the gyroscopic effect predicted for the simplified model actually does not occur.

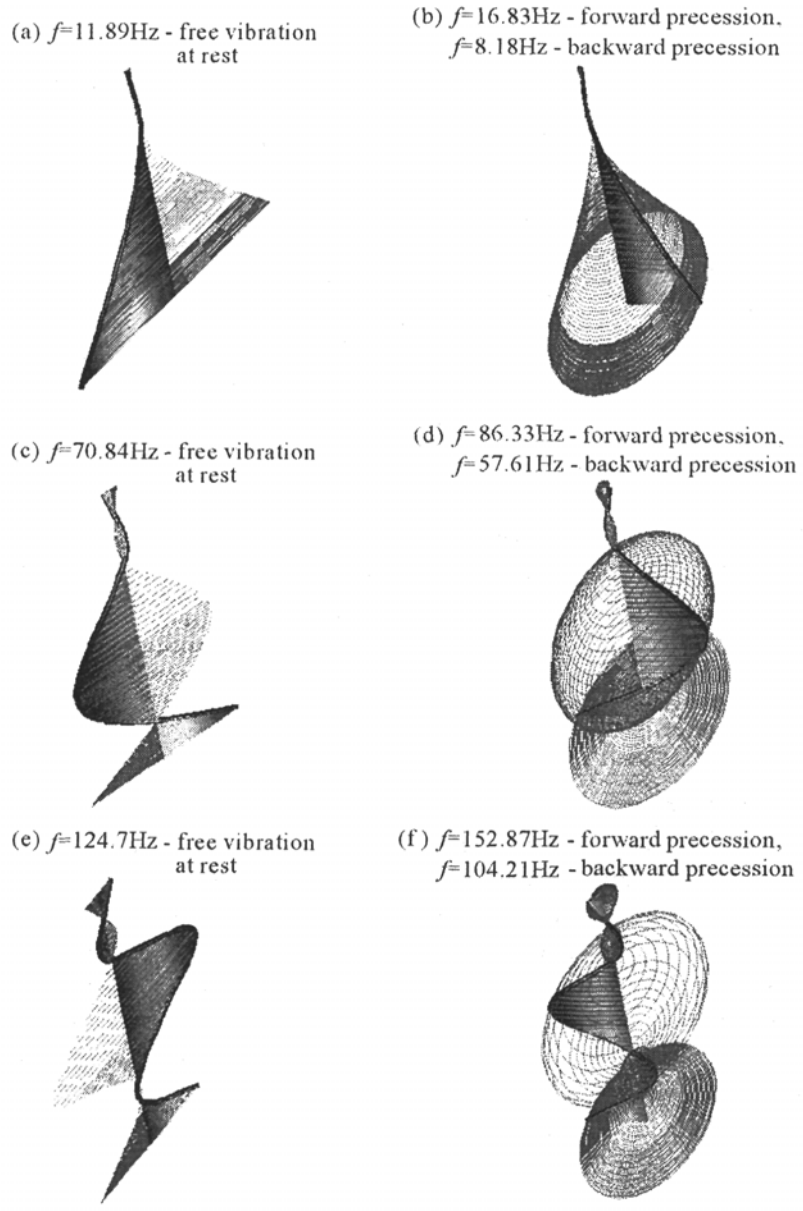

Fig. 9. Modal shapes and natural frequencies of the rotor for forward and backward precession

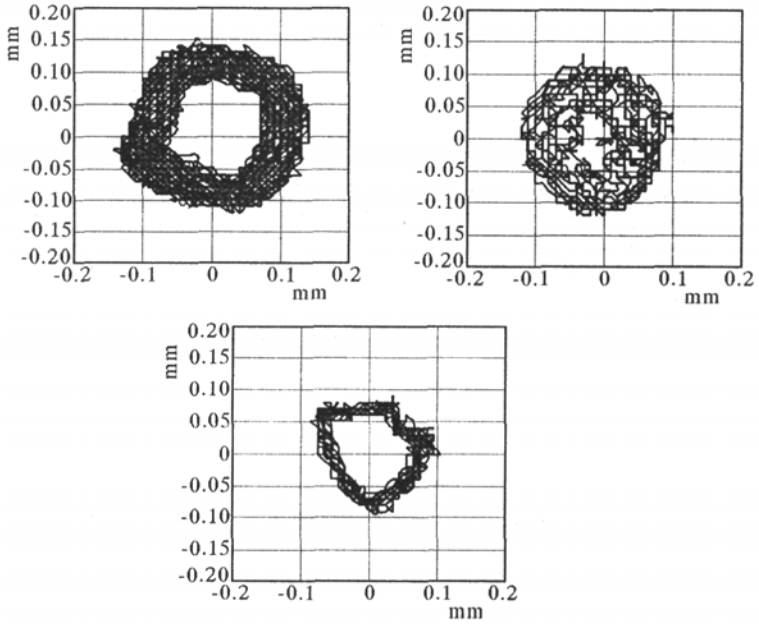

Fig. 10. Trajectories of a point lying on the shaft axis in the measurement section A-A (Fig. 1a) recorded in three centrifuges ACWW 1000

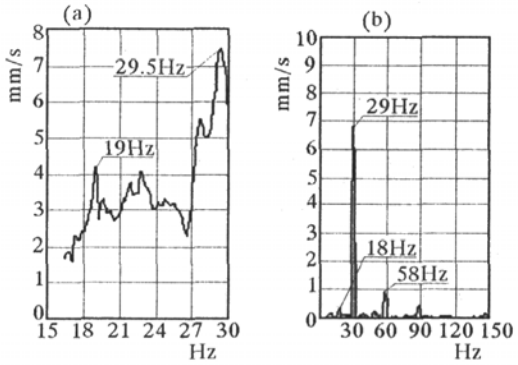

Fig. 11. Amplitude-frequency characteristics of the vibration velocity: (a) during rotor's run-up and (b) at the rotation frequency 30 Hz

High values of the amplitude in the velocity amplitude-frequency spectrum determined during the centrifuge operation with the rotational speed 29 Hz confirms the resonance character of vibrations in such conditions. A distinct amplitude that appears in the spectrum near the frequency 58 Hz, being the next forced frequency harmonic, proves the occurrence of the effect of clearances in the bearing system.

The presented analysis of the usefulness of the classic Green-Stodola's model for the description of the centrifuge rotor vibration confirms its imperfectness as we can only evaluate the basic free vibration frequency of a modeled real system. Although in the tested range of rotational speeds, the disk vibrations are not of great importance, which could justify the usage of a simple model treating the disk as an element with infinitely big stiffness, the discrepancy in the results related to precession effects forces one to be careful with such treatment of this problem. The possibility of formulation of sample matrices occurring in the system of equations of motion, including especially the gyroscopic matrix, is not always followed y correctness of achieved results due to their integration.

Acknowledgment

The authors express gratitude to the MSC Software company for rendering their accessible software used for calculations.

References

1. AWREJCEWICZ J., KRYSKO W.A., 2000, *Vibration of Continuous Systems*, WNT Warszawa
2. GOSIEWSKI Z., MUSZYŃSKA A., 2000, *Dynamics of Rotor Machinery*, Lectures collection, WSI Koszalin
3. GRYBOŚ R., 1994, *Dynamics of Rotors Machinery*, PWN Warszawa
4. JEI Y.G., LEE C.W., 1993, Modal characteristics of asymetrical rotor-bearing systems, *Journal of Sound and Vibration*, **162**, 2, 209-229
5. KANG Y., SHEEN G.J., WANG S.M., 1997, Development and modification of a unified balancing method for unsymmetrical rotor-bearing systems, *Journal of Sound and Vibration*, **199**, 3, 349-368
6. MIKOŁAJCZAK P., LIGIER K., 2003, Method of identification of critical damage states on the example of sugar centrifuge, *Diagnostic*, **29**, 53-60
7. MOHIUDDIN M.A., KHULIEF Y.A., 1999, Coupled bending torsional vibration of rotors using finite element, *Journal of Sound and Vibration*, **223**, 2, 297-316
8. NELSON H.D., MCVAUGH J.M., 1976, The Dynamics of rotor bearing systems using finite elements, *Journal of Engineering for Industry*, **98**, 593-599
9. SAWICKI J.T., GENTA G., 2000, Modal uncoupling of damped gyroscopic systems, *Journal of Sound and Vibration*, **244**, 431-451

10. ZACHWIEJA J., 2002a, Gyroscopic effect in paper machine cylinders dynamics, *Scientific Collection ATR, Mechanical*, **53**, 310-323

11. ZACHWIEJA J., 2002b, Vibrations of KL63 sheet cut guide cylinder, *Scientific Collection ATR, Mechanical*, **52**, 144-153

12. ZACHWIEJA J., 2004, Analysis of dynamics of Stodola-Green rotor in flexible bearing, *Developments in Machinery Design and Control*, **3**, 95-106

Analiza numeryczna dynamiki wirnika pionowego wirówki ACWW 1000

Streszczenie

W pracy przedstawiona została analiza dynamiki wirnika przewieszonego w ujęciu numerycznym. Obiektem rzeczywistym, który posłużył do weryfikacji zastosowanego modelu, był pionowy wirnik wirówki ACWW 1000, który z uwagi na cechy konstrukcyjne powinien wskazywać podatność na wpływ efektów żyroskopowych.

Manuscript received December 7, 2004; accepted for print January 31, 2005